- Impact on the Formation and Catalytic Property of
- 2 Pt based Nanocatalysts by Galvanic Reaction with

Co-reduction Agents

- 4 John R. Crockett^a, Maggie Wang^a, Joseph E. Doebler^a, Tejal Pawale^b, Xiao Li^b, Ying Bao^a*
- 5 ^a Department of Chemistry, Western Washington University, Bellingham, WA 98225, USA.
- 6 b Materials Science and Engineering Department, University of North Texas, Denton, TX 76207,
- 7 *USA*;

- * Email: ving.bao@wwu.edu
- 9 **ABSTRACT**. It has been shown that controlling the morphology and composition of Pt based 10 nanocrystals can effectively enhance catalytic properties. We report a detailed study on the impact 11 of using co-reducing agents in the galvanic replacement reaction (GRR) between Ag shell 12 templates and Pt precursors to better control the morphology, composition, and resulting 13 performance of the fabricated Pt based catalysts. Mesoporous silica supported silver shell coated 14 gold nanodumbbell nanostructures (AuNDB@Ag@mSiO₂) are synthesized via reducing silver 15 ions which have penetrated through the mSiO₂ layer and then be deposited on the surface of the 16 AuNDBs. These are used as templates and the morphology and optical properties of these templates can be adjusted by altering the amount of Ag⁺ in the depositing condition. The mSiO₂ 17

- layer shows some flexibility and does not influence the silver shell formation on the surface of
- 2 AuNDBs. Additionally, the thickness of the silver shell of the template and the strength of the
- 3 reducing agent used in the GRR impact the morphology, composition, and catalysis performance
- 4 of the resulting Pt based catalysts. A plausible mechanism on those observations is studied and
- 5 discussed.

6 INTRODUCTION

- 7 Platinum (Pt) based materials have been extensively used as catalysts in a wide range of reactions
- 8 including catalytic conversion, hydrogenation, oxidation, and reduction. However, Pt is
- 9 expensive and has limited reserves, resulting in drawbacks of utilizing Pt for various applications.
- 10 Thus, a wide range of many experimental and theoretical studies have been motivated by
- developing approaches to maximize Pt's catalytic performance.
- In general, increasing the surface area of Pt as well as integration with other metals (e.g. Pd, Au,
- 13 Ag, Fe, Cu) to form alloyed or multiple-component metallic nanomaterials are two effective
- 14 approaches to improving Pt's catalytic performance. For example, Nørskov group used density
- 15 functional theory to study various aspects of Pt based metal clusters on oxygen reduction reactions
- 16 for fuel cells.⁵ Adzic group and Stamenkovic group reported many studies of Pt or Pt-bimetallic
- monolayers or multilayers on supported substrates for fuel cells and their experimental results are
- often supported by computational work from Mavrikakis group. 6-8 Pt or Pt alloy metal clusters
- deposited on film or other supported surfaces have also been studied by Brankovic, Shao, M., and
- 20 Dimitrov groups. 9-13 Although systems including synthesizing freestanding small sized
- 21 nanoclusters or depositing metal atoms on the substrate have shown significant progress, they have
- their own drawbacks such as tending to sinter (form bigger particles) or dissolving due to their
- small particle instability as well as detaching from their supporting surface. 14-17

An alternative system that focuses on fabricating self-stabilized Pt based colloidal nanoparticles has also received a lot of attention. So far, significant progress has been made in colloidal nanoparticles system toward this goal, though key challenges remain. One approach to enhancing Pt's catalytic performance has focused on synthesizing Pt nanostructures with controlled morphologies. ¹⁸⁻¹⁹ El-Sayed and co-workers demonstrated that the shape of platinum nanoparticles affected their catalytic activity toward the reduction of hexacyanoferrate.²⁰ Their study demonstrated that there was a direct relationship between the percentage of available edge or corner sites and the catalyst activity among various shapes of Pt resulting in the highest activity with the tetrahedral catalysts (the most edge and corner sites). More generally, hollow structures, porous structures and dendrite structures have large specific surface areas and enormous active sites.²¹⁻²³ A second approach to improve Pt's performance for various electrocatalytic reactions has been to introduce other metals (e.g. Au, Ag, Fe, Cu) to Pt and form alloyed or multiplecomponent metallic nanomaterials.²⁴⁻²⁶ Pt based heterogeneous metallic nanocrystals have shown enhanced catalytic properties in comparison with pure Pt nanocrystals due to a strong electronic coupling between the metals.²⁷ Combining these two approaches by developing methods to synthesize Pt based multi-metallic nanocrystals with large surface area is a promising direction for additional improvements in catalytic performance, as discussed in a number of studies.²⁸⁻²⁹ Strategies to obtain a high surface area of Pt such as sequential reduction of platinum on top of a particle template with large surface area or reduction of platinum on top of a particle with post treatment are effective. 30-31 However, galvanic replacement reaction (GRR) has emerged as one of the most popular synthesis.³²⁻³⁵ It offers a unique advantage in that it can create platinum based multi-metallic nanostructures whose shape, 35 size, 35 and composition 36 can be precisely controlled without the

1

2

3

4

5

6

7

8

9

10

11

12

13

14

15

16

17

18

19

20

21

22

need for post-synthetic modifications (annealing) or an applied potential. Hollow Pt-Ag nanocatalysts, obtained via simple GRR between a Pt precursor and sacrificial Ag templates, have been commonly synthesized and were pioneered by Xia group. 37-40 Their recent study has also demonstrated that Pt/Ag nanocatalysts have great catalytic performance for oxygen reduction reactions.³⁷ The GRR can be coupled with co-reduction by introducing a reductant into the galvanic replacement reaction. With the addition of the secondary reducing agent, the shape and composition of the resulting nanostructure can be manipulated beyond what can be achieved in the simple galvanic replacement as the secondary reducing agent introduces new pathways and products to the reaction. To fabricate desire nanostructure, one must carefully control both the rates of co-reduction and GRR. For example, the Xia group has successfully synthesized Pd-Pt nanocages with greatly enhanced catalytic activities by coupling the GRR between Pd nanocubes and K₂PtCl₄ with a co-reduction process by using citric acid as the reductant.⁴¹ Although the Xia groups' nanostructures have displayed excellent catalytic properties, Pd is another expensive metal in the Platinum family. Thus, using Pt and a relatively cheaper metal for the GRR would be beneficial and silver has been frequently preferred because of its very low redox potential. 42-44 However, there are only a few reports demonstrating the use of both Ag templates/Pt precursors and co-reduction in a GRR to generate Pt based nanostructures. 45-46 Camargo group studied the different impact on the morphology of synthesized AgPt nanomaterial when performing GRR with and without a co-reduction agent. 45-46 To the best of our knowledge, there are no reports studying in detail on the impact of reduction agents on fabricating Pt based nanocatalysts via the galvanic replacement approach with Ag template. Additionally, there is a lack of understanding on the effect

1

2

3

4

5

6

7

8

9

10

11

12

13

14

15

16

17

18

19

20

21

of the catalytic performance due to the resulting morphology and composition of the nanostructures.

In this paper, Pt based catalysts are obtained using GRR coupled with co-reducing agents between Ag shell templates and Pt precursors. The Ag shell template are created by first synthesizing a mesoporous silica (mSiO₂) shell supported gold nanodumbbell (AuNDB) nanostructure, where the mSiO₂ stabilizes the nanostructure for further treatment. Due to the porosity of the mSiO₂ shell, silver ions will penetrate the shell and deposit on the surface, forming the AuNDB@Ag@mSiO₂ template for GRR. The morphology of this template (specifically the thickness of the silver shell) will also be able to be adjusted by altering the amount of Ag⁺ used. With the fabricated AuNDB@Ag@mSiO₂ nanostructures, hydroquinone and ascorbic acid will be separately used as reducing agents to assist the galvanic replacement reaction between the Pt precursor and Ag sacrificial template. Varying the thickness of silver shell and the strength of the reducing agent will impact the rates of co-reduction and GRR in the system and will affect the final morphology and composition of the Pt based catalysts. The mechanism of catalyst formation is proposed and supported with evidence from further characterization. The catalytic performance of the resulting Pt based catalysts was evaluated in the reduction reaction of 4-nitrophenol to 4aminophenol. The relationship between the morphology and composition of nanostructures and their catalytic performance, as well as the proposed mechanism behind this, are discussed.

RESULTS AND DISCUSSION

3

4

5

6

7

8

9

10

11

12

13

14

15

16

17

18

19

20

21

22

23

Creation of AuNDB@Ag@mSiO₂ nanostructures for the use as GRR template. Following the process illustrated in Figure 1a, mesoporous silica shell supported AuNDB@Ag nanostructures (AuNDB@Ag@mSiO₂) were created for later use as templates in a galvanic replacement reaction where Pt²⁺ is added. The synthesized products from each step in this process were characterized

1 via scanning transmission electron microscopy (STEM) and representative results are shown in 2 Figure 1b-e. Initially, gold nanorods (AuNRs) with aspect ratio 3.8 ± 0.6 were first synthesized using a previously published method, with representative results shown in Figure 1b. 47-48 Next, 3 4 AuNDBs were formed based on iodide-mediated growth using synthesized AuNRs as seeds, and 5 the formation mechanism is discussed in more detail in the supporting information (SI).⁴⁹ 6 Comparing to the AuNR seeds, the resulting AuNDBs will have increased aspect ratios 5 ± 2 , 7 which can be noticed in Figure 1c, a representative STEM image of AuNDBs. It is worthwhile to 8 mention that the samples are not 100% AuNR and AuNDBs; there are some by-products such as 9 spheres resulting from the synthesis process. These AuNDBs were then coated with a layer of 10 mesoporous silica shell (AuNDB@mSiO₂), as discussed in detail in the Experimental Section. 11 Figure 1d shows a representative STEM image of the resulting nanoparticles and the formed 12 mSiO₂ shell thickness is approximately 19 nm, which were measured on either side of AuNDBs. 13 A layer of silver shell was created via a reduction process of AgNO₃ near the surface of the 14 AuNDBs to form AuNDB@Ag@mSiO2, which altered the shape of the nanostructures from 15 dumbbell-like back to a rod-like shape, representative results of which are shown in Figure 1e. 16 Note that the exact shape will depend on the amount of AgNO₃ added, which will be discussed in 17 more detail later. This indicates that the silver ions can penetrate through the silica shell due to its 18 porosity and be reduced on the surface of Au. In addition, this demonstrates that the mSiO₂ shell 19 is flexible to some extent because the shell, previously dumbbell shaped, changed to a rod-like 20 shape due to the swelling force from the enlarged core. The optical properties of the products of 21 each of these steps were also monitored. The results are shown in Figure S1 along with a detailed 22 discussion.

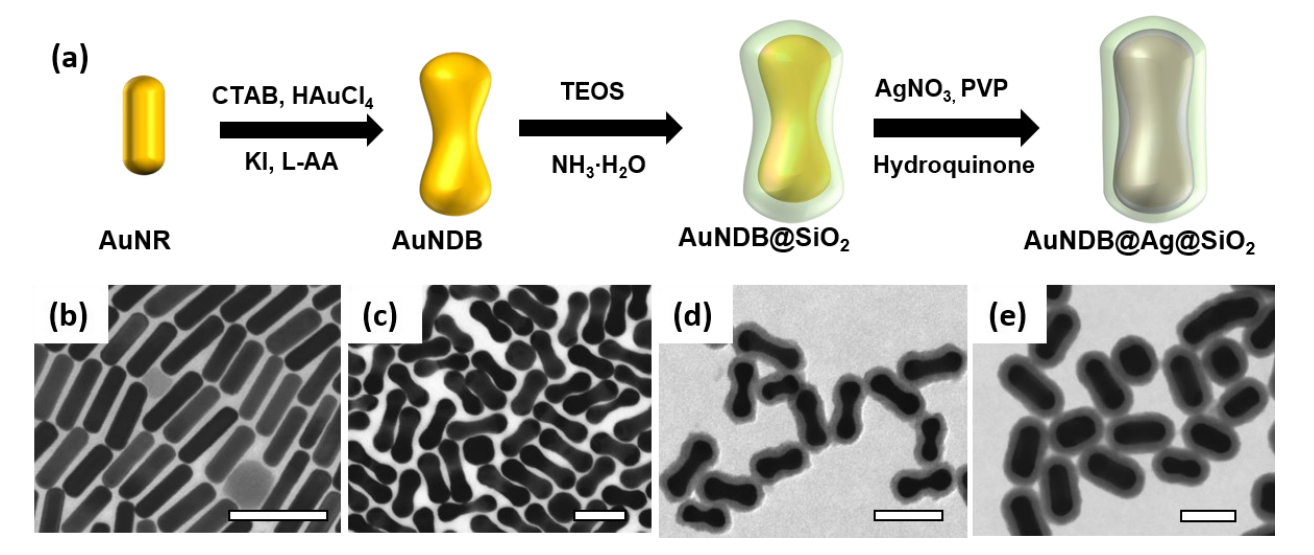


Figure 1. (a) Illustration of synthesis of a mesoporous silica shell supported AuNDB@Aq nanostructure. (b-e) STEM images of (b) gold nanorods (AuNRs), (c) gold nanodumbbell (AuNDB), (d) gold nanodumbbell@silica (AuNDB@mSiO₂) and (e) silver deposited gold nanodumbell@silica (AuNDB@Ag@mSiO₂). Scale bar: 100 nm. 5

2

3

4

6

7

8

9

10

11

12

13

14

15

16

17

The synthesized AuNDB@Ag@mSiO₂ was further studied to better understand the silver deposition process on AuNDB@mSiO₂. Figure 2a is the STEM image obtained by combining bright field and high-angle annular dark-field (HAADF), demonstrating the details of the nanostructures. The bright area on the nanostructures are the silica shells while the darkest areas on the nanostructures are the AuNDBs. The Ag appears as lighter grey thin layers surrounding the AuNDBs. This shows that the silver layer is thicker in the center of the dumbbell structure while become thinner toward the tips. To further confirm the deposition sites of the Ag atoms on AuNDB@Ag@mSiO₂, HAADF-STEM and energy-dispersive X-ray (EDS) were performed to examine the spatial distribution of Ag and Au on a single nanostructure (Figure 2b). The HAADF-STEM image is shown in the first panel of Figure 2b. Since the HAADF-STEM image is formed by collecting the scattered electrons, silica does not appear in the image due to its low atomic number and weak electron interaction, while gold and silver appear bright in the image due to their

higher atomic number and stronger electron scattering. The corresponding elemental mappings (second and third panel of Figure 2b) clearly show the presence of Ag as a shell surrounding the Au atoms. The map of Ag atoms show less silver on the tips of the rod structures, while most Ag atoms are located on the center of the dumbbell structure, which agrees with STEM results in Figure 2a. The preferential silver reduction at the central area of the AuNDBs or Au NRs instead of the tips has been also observed by others in a similar deposition process that did not involve a silica shell. 50-51 It is known that silver overgrowth takes place preferentially at the high-energy facets, including <100> and <110>, which tends to reduce the free surface energy. 52-53 Since the <100> and <110> are richly located on the lateral side, not on the tip of AuNDBs or Au NRs, silver deposition preferentially takes place on its lateral facets. 51

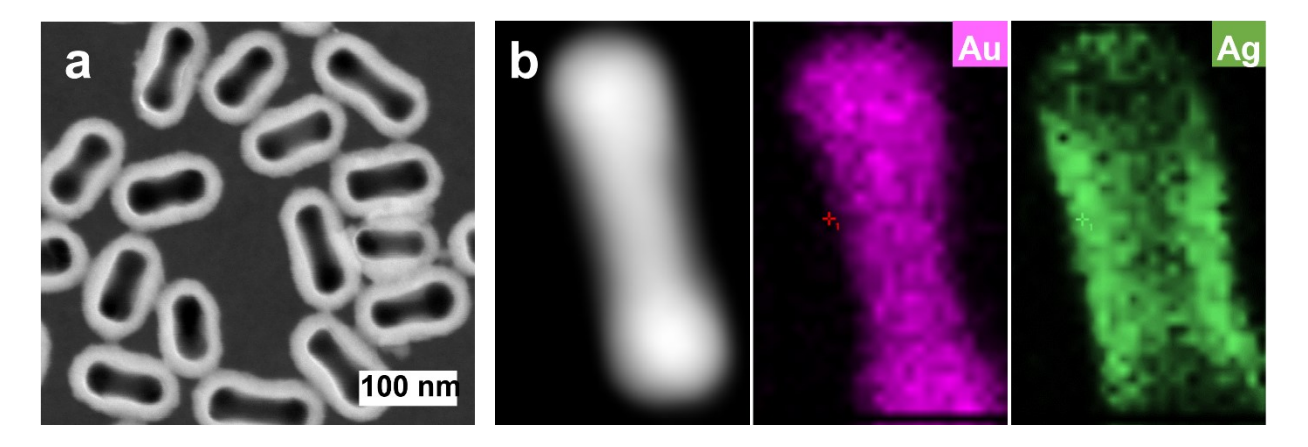


Figure 2. (a) STEM image of AuNDB@Ag@mSiO₂, (b) HAADF-STEM and elemental mapping of one AuNDB@Ag@mSiO₂. The pink and green colors in the elemental maps stand for gold and silver, respectively.

Figure 3 depicts representative STEM images of AuNDB@Ag@mSiO₂ nanostructures when varying volumes of AgNO₃ were used in the Ag deposition process. The morphology of the AuNDB@Ag@mSiO₂ changes with increased Ag⁺ ion concentration in the growth solution. At the lowest volume of AgNO₃ (10 μL, shown in Figure 3a), the Ag shell seems quite thin and the

Ag mainly reduced at the central area of the AuNDBs, keeping the silica shell in a dumbbell like shape. As volume increases to 20, 30, and 40 μL, the Ag shell becomes thicker and the enlarged Ag shell pushes the encompassing silica shell outward, taking on a cylindrical rod shape (shown in figure 3b-d). When the volume of AgNO₃ increases further from 50 μL to 200 μL, an anisotropic Ag coating occurs, which results in increased width of the nanoparticle and an irregularly shaped AuNDB@Ag. This anisotropic growth process is consistent with previously reported silver deposition on silica shell-free gold nanorods, indicating that the mSiO₂ shell did not influence the NP growth behavior.⁵⁴ In addition, we can observe in Fig 3d-i that the mSiO₂ shell becomes thinner and eventually breaks under high volumes of silver deposition, which is the result of the swelling force from the enlarged NPs. This result clearly demonstrates that the mSiO₂ shell is not rigid; instead, it is elastic to some extent. It allows the growth of AuNDB@Ag while still supporting the enlarged AuNDB@Ag with tension. The elastic characterization of mSiO₂ shell at extremely thin thickness will be of great interests to explore the reversibility and adaptability of irregularly shaped mSiO₂ shell in our future work, which is beyond the scope of this current work.

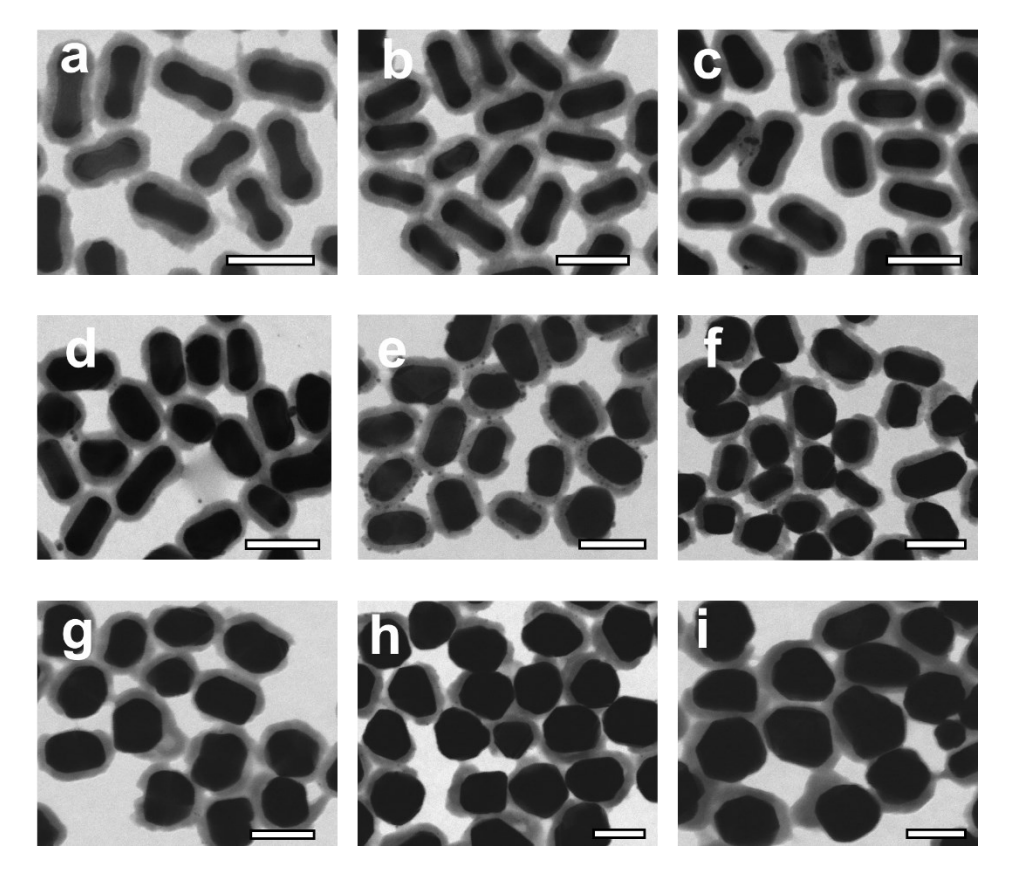


Figure 3. STEM image of AuNDB@Ag@mSiO2 with varying volume fractions of silver obtained by adding different amounts of a 10 mM silver nitrate solution: (a) 10 μL, (b) 20 μL, (c) 30 μL, (d) 40 μL, (e) 50 μL, (f) 60 μL, (g) 100 μL, (h) 120 μL, and (i) 200 μL. Scale bar: 100 nm.

Optical properties can be also tailored by forming silver shells with various thickness on the surface of the AuNDBs. The AuNDB@mSiO₂ without silver coating (0 µL of AgNO₃) has the LSPR peak located at 830 nm. With the progressively increased volume, it is clearly observed from Figure 4a that the LSPR peak undergoes a continuously blue shift. Eventually, with 200 µL of AgNO₃, the LSPR is merged with other peaks and forming a broad peak which is understandable as the silver content is very high and causing the nanostructure to take an irregular sphere shape. The peak positions of all the samples have been fitted and found to obey exponential decay

behavior, as shown in Figure 4b. Note: the LSPR peak position of sample from 200 μ L is estimated since it is not a distinguishable separated peak. It is necessary to mention that the additional silver deposition is crucial in observing a wide shift in LSPR peak position. The corresponding photo of nanoparticle solution in the inset of Figure 4b demonstrates the effect of increased silver content on the solution color. Moving from low to high silver content, the solution color changes from light red to muddy orange.

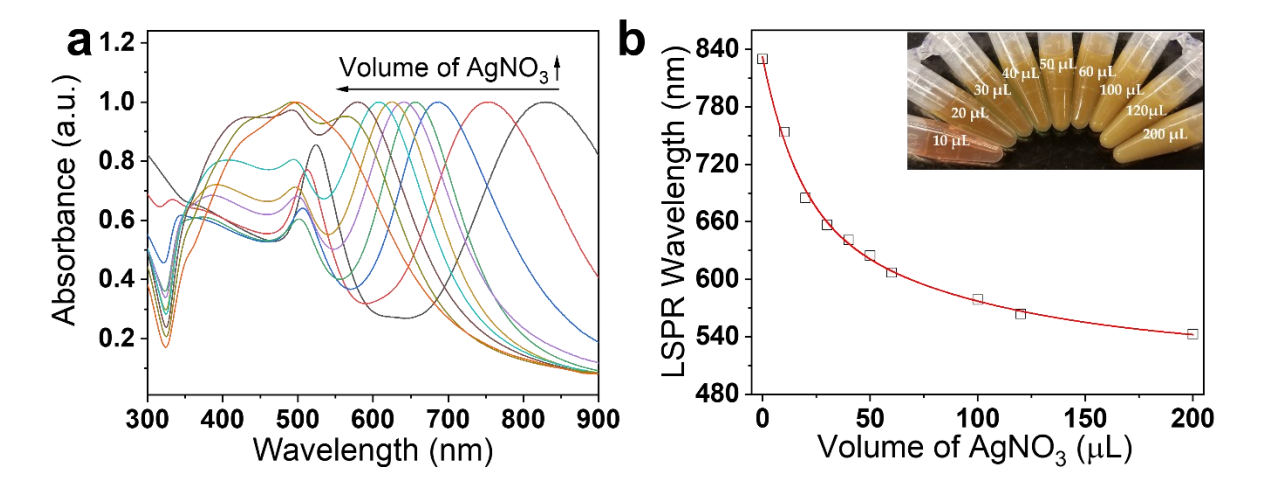
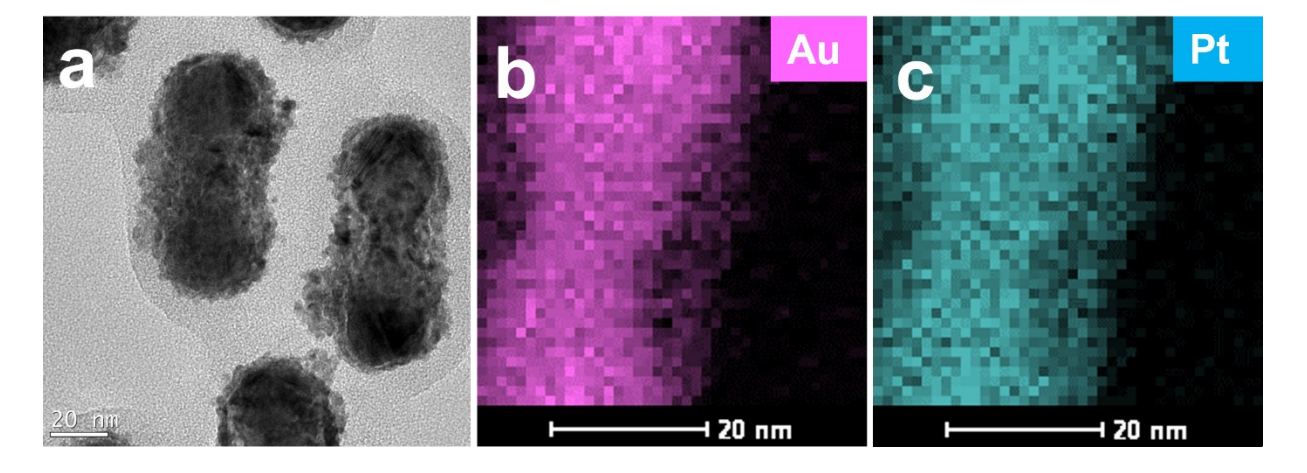


Figure 4. (a) UV-Vis absorption spectra of AuNDB@Ag@mSiO2 nanostructures with varying volume fractions of silver obtained by adding different amounts of a 10 mM silver nitrate solution: (from right to left spectra) 0 μL, 10 μL, 20 μL, 30 μL, 40 μL, 50 μL, 60 μL, 100 μL, 120 μL, and 200 μL, respectively. (b) LSPR peak location as function of silver nitrate solution volume; (insert) color changes as the silver nitrate volume increases.

Reducing agent assisted galvanic replacement for the formation of Pt based nanocatalysts.

The Ag shell of the silica shell supported AuNDB@Ag nanostructure created in the prior section is used as a sacrificial template to guide the formation of Pt via the GRR between the Ag shell template and the Pt precursor. During the GRR, the reducing agents, hydroquinone (HQ) and ascorbic acid (AA), are used and their impact on the morphology formation are studied.

Transmission electron microscopy (TEM) image (Figure 5a) shows the detailed morphology of the nanomaterial obtained by using HQ as co-reducing agent and K₂PtCl₄ as Pt precursor to react with AuNDB@Ag@mSiO₂ nanostructures made with 20 μL of AgNO₃. The resulting nanocatalysts maintained a full silica shell coating. The metal nanostructure retained a dumbbell shape for its core but the shell became a hollow structure with a rough surface formation instead of a uniform silver layer. EDS was performed to examine the spatial distribution of the metal elements on a single nanostructure and the results are shown in Figure 5b and c. The Au element distribution shows the AuNDB still maintains the dumbbell shape. The hollow structure appears to have Pt elements. Ag was not able to be detected and this result is omitted from Figure 5. This indicates that Ag shell is fully replaced by Pt via the co-reduction galvanic replacement reaction. The UV-Vis spectra of nanostructure before and after the galvanic reaction are shown in Figure S2. From the spectra, it can be noted that the silver peak at 340 nm (indicated with red dashed circle) is barely recognizable after the galvanic reaction which supports the EDS results. Additionally, the LSPR has a red-shift to 820 nm which is closer to the LSPR of AuNDB@Ag@mSiO₂ nanostructures (830 nm), indicating the absence of plasmon coupling effect from Ag shell.



1

2

3

4

5

6

7

8

9

10

11

12

13

14

15

- 1 Figure 5. (a) TEM image of HQ assisted Pt based nanocatalyst using
- 2 AuNDB@Ag@mSiO₂ made with 20 μL of AgNO₃ (Ag/Pt = 2/2), (b)-(c) elemental mapping
- 3 of one galvanic reacted metal nanostructure. The pink and blue colors in the elemental
- 4 maps stand for Au and Pt, respectively. Ag result omitted due to non-detection.
- 5 The same HQ assisted galvanic reaction was the performed with all the AuNDB@Ag@mSiO₂
- 6 made with different amount of silver content, as discussed in the previous section. The calculated
- 7 Ag/Pt molar ratios for all the AuNDB@Ag@mSiO₂ are x/2, where x=1, 2, 3, 4, 5, 6, 10, 12, and
- 8 20. Throughout this manuscript, Ag and Pt concentrations will be described as molar ratios
- between Ag and Pt; their galvanic replacement reaction is: $PtCl_4^{2-} + 2Ag \rightarrow Pt + 2Ag^+ + 4Cl^-$ which
- shows that in order to replace all the Ag present without a co-reducing agent, it requires a Pt/Ag
- 11 ratio of 1/2. It also indicates that samples with a Ag/Pt molar ratio more than 4/2 will not be fully
- 12 galvanically reacted in the absence of a co-reducing agent.
- Representative STEM images of resulting nanostructures with various Ag/Pt molar ratios are
- shown in Figure S3a-i. Note the amount of Pt remains constant and only the Ag content is
- 15 changing. With the lowest molar ratio (Ag/Pt=1/2), it can be observed that the hollow shell
- structure is present with tiny gaps between the shell and the AuNDB core. In addition, there are
- 17 numerous spiky features on the hollow structure. These spiky structures fade away as the molar
- 18 ratio increases. The space between the core and hollow shell is increased with increased molar
- 19 ratio. This is reasonable because the silver shell thickness increases with increased molar ratio.
- 20 During the galvanic reaction, the silver shell is the template metal which will be oxidized and
- 21 dissolved in solution while Pt, the oxidant metal, will be reduced onto the surface of the particle.
- Thus, the larger the particle is, the larger the volume of the shell will be.

Due to the observation of numerous spiky features on the hollow structure that formed from the lowest molar ratio (Ag/Pt=1/2) by HQ, a relative stronger reducing agent, AA, was selected to study the impact on the morphology formation of Pt based nanocatalysts via a stronger reducing agent assisted galvanic reaction. Initially, the galvanic reaction was carried out on AuNDB@Ag@mSiO₂ nanostructures made with 20 μL of AgNO₃. The UV-vis spectra (Figure S4) after the reaction is dramatically different from the one obtained before the reaction. The absorbance intensity is increased from the 0.2-1.0 range to the 1.0-1.5 range. Previously there were two large peaks, but after the reaction these were no longer able to be identified, and leaving only a small peak around 530 nm. This is also different from the sample obtained when using HQ reducing agent, as discussed earlier. The TEM image (Figure 6a) shows that the morphology of the synthesized sample using AA is significantly different from the one using HQ. The fabricated nanostructure does not show a clear hollow structure. Instead, there are a great number of spiky branches formed. It has been reported that the spiky branched features often results from kinetic control synthesis conditions where the reaction rate is slower than normal reaction, and the reduced atoms migrate to the surface of metal to form the spiky branches under the guidance of a "diffusion-limited aggregation" strategy. 23, 55 In our work, the kinetic control condition is formed by using relatively weak reducing agents (HQ and AA), the metal ions are reduced in solution and slowly migrate back to form the spiky branches. We believe that the mesoporous silica shell possibly affects how the metal atoms are transported to the deposition locations and form the unique spiky branches. The impact of silica shell for the kinetic controlled deposition process will be studied in the future. The EDS results in Figure 6b-d show that the Au element distribution exhibits the dumbbell shape. The silver element was distributed mostly on the shell surrounding the AuNDB, though it

1

2

3

4

5

6

7

8

9

10

11

12

13

14

15

16

17

18

19

20

21

22

also has relatively high atom intensity on the spiky branches, indicating that the formed branches are partly made of silver. The platinum element distributed across the whole nanostructure and the overall shape closely matches a combination of gold plus silver element distributions. It is worthwhile to mention that the spiky feature with relatively weak intensity in Au element map (Figure 6b) is an artifact due to the EDX peak overlap between Au and Pt. From this result, we believe that platinum is not only on the surface of nanostructure after the galvanic reaction but is also mixed with silver. The HRTEM helps to reveal the crystal information of the surface of nanostructure and further our understanding on the Pt and Ag formation as shown in Figure S5. The measured lattice spacings (Figure S5b) are ~ 0.23 nm which is larger than that of Pt(111) (0.226) nm) and smaller than that Ag (111) (0.236 nm), implying the generation of a Pt-Ag alloy. 56-57 To further support the formation of AgPt alloy, we performed X-ray photoelectron spectroscopy (XPS) measurement on the sample (Ag/Pt molar ratio = 3/2) prepared by AA assisted GRR to analyze the surface chemical composition. As shown in Figure S6, the peaks of Ag 3d5/2 and Ag 3d3/2 located at 367.38 and 373.21 ev indicate that the metallic state Ag⁰ is absolutely predominant in the composite. Meanwhile, there are two peaks at binding energies of 313.88 and 331.08 eV resulting from Pt 4d5/2 and 4d3/2 for the composites. A noticeable shift of the Pt 4d5/2 and 4d3/2 binding energy relative to that of pure Pt (315 ev for Pt 4d5/2 and 330 eV for Pt 4d3/2 indicated by green dash line) is probably due to the electron donation from Ag to Pt in the formation of AgPt alloy. Similar peak shifts of Pt energy peaks in AgPt alloy have been observed and reported from other works. 58-59 The same AA assisted GRR was performed with all the AuNDB@Ag@mSiO₂ made with different amounts of silver content, including the Ag/Pt molar ratios x/2, where x=1, 2, 3, 4, 5, 6, 10, 12, and 20. Representative STEM images of the resulting nanostructures with various Ag/Pt

1

2

3

4

5

6

7

8

9

10

11

12

13

14

15

16

17

18

19

20

21

22

molar ratios are shown in Figure S7a-i. They reveal that with low molar ratio Ag/Pt=1/2, 2/2, 3/2, and 4/2, the nanostructures not only have prominent spiky branches, but also the hollow shell structures are less obvious and uniform on individual nanoparticles. With the increased molar ratios, the spiky branches slowly fade out and the hollow shell becomes clear and larger with increased silver shell thickness.

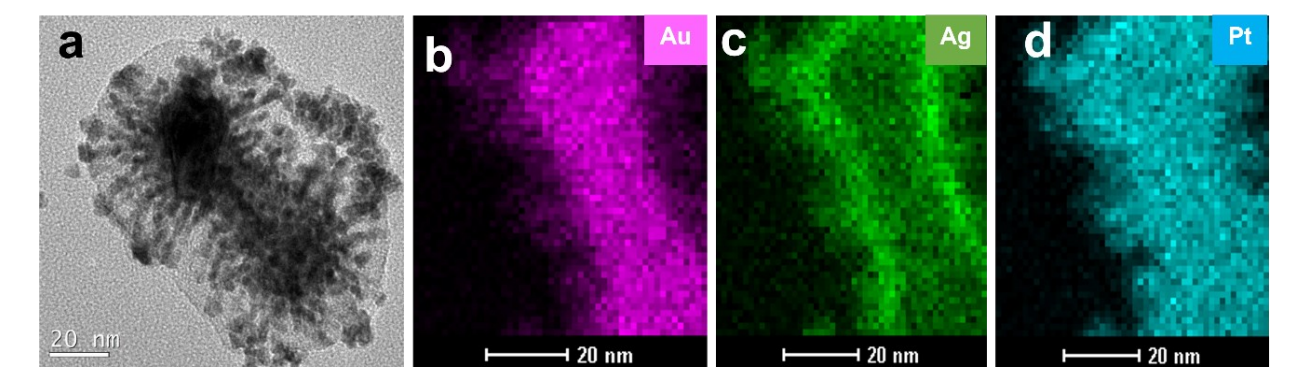


Figure 6. (a) TEM image of AA assisted Pt based nanocatalyst using AuNDB@Ag@mSiO2 made with 20 μL of AgNO₃ (Ag/Pt=2/2), (b)-(d) elemental mapping of one galvanic reacted metal nanostructure. The pink, green and blue colors in the elemental maps stand for Au, Ag, and Pt, respectively.

Mechanism of catalyst formation using reducing agents. Here, we propose a plausible mechanism that can account for the morphology changes under certain reducing agents and various Ag/Pt molar ratios. This mechanism should account for key results observed in our data and we review those in one place here. For the HQ system, 1) the nanocatalyst fabricated with molar ratio Ag/Pt=2/2 shows Au and Pt elements but Ag is undetectable; 2) the hollow shell formation is clearly observed within all the nanocatalyst samples; 3) the nanocatalyst fabricated with the lowest molar ratio (1/2) appears to have fuzzy spikes on the surface of the shell. However, as the molar ratio increased, the fuzzy spikes quickly fade out -- for example, it is difficult to observe them even in the sample fabricated with a molar ratio of 2/2. In addition, the shell volume increases with

1 increased molar ratio. For the AA system, 1) the nanocatalyst fabricated with molar ratio 2 Ag/Pt=2/2 shows Au, Ag, and Pt elements and the HRTEM indicates the Ag-Pt forms an alloy on the surface of nanostructure; 2) the hollow shell structures are less obvious for low molar ratio 3 4 samples such as Ag/Pt=1/2, 2/2, and 3/2; 3) the nanocatalyst fabricated with relatively low molar 5 ratio (1/2, 2/2, 3/2, 4/2) appears to have spiky branches on the surface of the shell and with higher 6 molar ratios, they slowly disappeared. In addition, the shell volume increases with increased molar 7 ratio. 8 There are four possible reactions involved in the process. 1) the galvanic replacement between Ag and $PtCl_4^{2-}$ (Reaction: $PtCl_4^{2-} + 2Ag \rightarrow Pt + 2Ag^+ + 4Cl^-$); 2) the reduction of $PtCl_4^{2-}$ by a 9 reducing agent (Reaction: PtCl₄²⁻ + Reducing Agent → Pt + 4Cl⁻); 3) the reduction of produced 10 Ag^+ by a reducing agent (Reaction: $Ag^+ + Reducing Agent \rightarrow Ag$); and 4) the formation of AgCl 11 precipitate if the concentrations of Ag^+ and Cl^- are high enough (Reaction: $Ag^+ + Cl^- \rightarrow AgCl$). 12 The galvanic reaction, reaction (1), will lead to the formation of a hollow structure 43, 60-61, whereas 13 14 the reduction by reducing agent will result in the formation of a spiky branches shell on the 15 AuNDB@Ag@mSiO₂ nanostructure mainly due to kinetic controlled deposition process... 16 Reactions (2) and (3), the reductions by the reducing agent, compete with reaction (1), the galvanic 17 replacement. The standard redox potential of $PtCl_4^{2-}/Pt$ (+0.76 V) is lower than that of Ag^+/Ag (+0.8 V) which 18 19 allows the galvanic reaction to occur. For the reducing agents, the redox potential for HQ is E°=0.7 V, and for AA is $E^{\circ}=0.35 \text{ V}$. The more positive the potential is, the greater the species' affinity 20 21 for electrons and the more the species tends to be reduced. From this, we know that the AA has more positive potential, which means stronger reducing ability, in terms of reducing PtCl₄²⁻ to Pt 22 and Ag⁺ to Ag than HQ has. From the redox potential values of the key species and the observed 23

previous results, we infer that the HQ has weak or no reducing capability in this context, which results in weak or no parallel reduction by HQ when competing with the galvanic reaction. In contrast, the AA has strong reducing power which can be clearly observed due to the Ag/Pt alloy spiky branch formation previously discussed. The reaction rates of the competing reactions can be controlled by the concentration of AA and Ag. In our case, the reaction pathway is controlled by keeping the reduction rate (R_{red}) constant and manipulating the galvanic rate (R_{gal}) by varying the silver shell thickness and hence the obtained morphology of final product. When the silver shell is relatively thin, the reducing reaction will dominate while the galvanic reaction barely takes place. In this case, part of the PtCl₄²- is reduced by the reducing agent into a Pt atom and epitaxially deposits on the surface of the Ag nanoparticle to form the incomplete thin Pt shell. Meanwhile, PtCl₄²- can oxidize a small part of the Ag shell through galvanic replacement. The Ag⁺ produced by the galvanic replacement can also be reduced by AA and then deposit on the newly formed Pt layer, forming a porous Ag-Pt alloy shell. Due to the porous structure of silica shell, the Ag-Pt alloy structure becomes spiky branches as illustrated in Figure 7 (top panel) and the experimental results in Figure S7a. In the case of a thick silver shell, the galvanic replacement reaction would be faster than reduction reaction of AA. As a result, the inner Ag shells are totally removed by galvanic replacement and the hollow porous Pt shells are built as illustrated in Figure 7 (bottom panel) and the experimental results in Figure S7i.

1

2

3

4

5

6

7

8

9

10

11

12

13

14

15

16

17

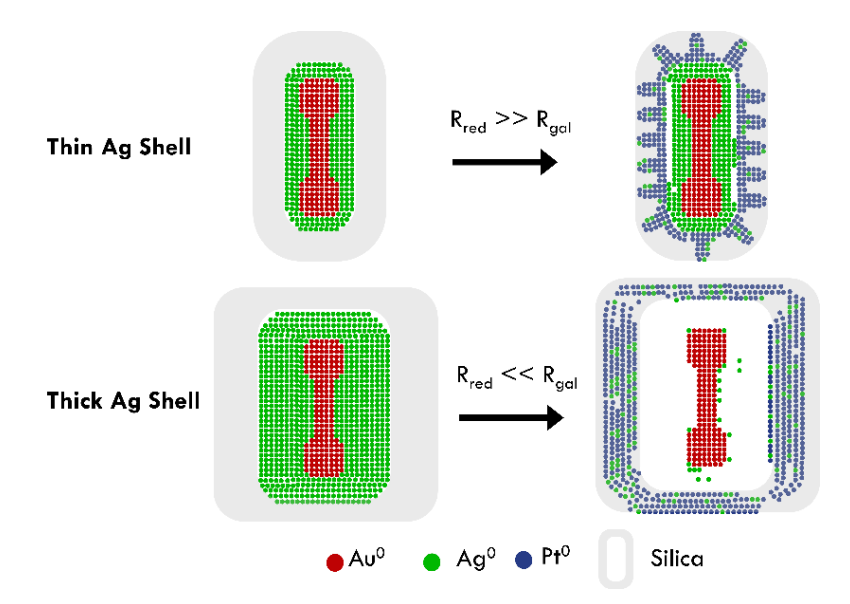


Figure 7. Schematic illustration of the two possible routes and products for synthesis that involve Ag shell and Pt precursor in the presence of thin and thick silver shells under AA assisted GRR system.

The R_{gal} can be investigated by collecting the UV-visible spectra during the reaction at different times. In this case, the UV-visible spectra during the reaction on samples with molar ratio of Ag/Pt = 3/2 and 5/2 were collected separately over 15 min intervals, as shown in Figure S8a and b. From the spectra, it is clear that the sample with Ag/Pt molar ratio = 3/2 has substantially more separated spectra than the sample with Ag/Pt molar ratio = 5/2, which indicates that the reaction on the sample with Ag/Pt molar ratio = 3/2 takes longer to complete as compared to the reaction in the sample with Ag/Pt molar ratio = 5/2. In addition, during the reaction process, the peak initially located at 510 nm shows a gradual shift in both wavelength and intensity and eventually does not change further, which indicates the reaction is complete. The intensity value of this peak was then analyzed and plotted as a function of reaction time, shown in Figure S8c. It is very clear that the sample with Ag/Pt molar ratio = 5/2 takes a much shorter time to reach the maximum intensity and

1 to complete the reaction. This is evidence that the R_{gal} will increase with increased Ag/Pt molar 2 ratios, which in this context means thicker silver shells. To support the hypothesis that the Ag⁺ ions were reduced by AA, one item of evidence is that 3 4 with a higher molar ratio, there are no AgCl crystals observed. The representative SEM image 5 (Figure 8a) of the sample with highest molar ratio (Ag/Pt=20/2) shows that no big crystal appears. 6 Under EDS, there are no Cl elements that can be detected, shown in Figure 8b and Figure S9a. To confirm that AA also reduced PtCl₄²⁻ to Pt, all samples were studied by EDX and the atomic ratio 7 8 of Ag/Pt was plotted against the volume of silver nitrate in Figure S10. Reaction (1) shows that to 9 complete the galvanic replacement, the Ag/Pt molar ratio must be at least 4/2. This indicates that 10 a Ag/Pt molar ratio less than 4/2, such as 1/2, 2/2, or 3/2, will not have a complete galvanic replacement. If that is the case, there should have been excess PtCl₄²⁻ in solution. However, from 11 12 the EDX results, samples from Ag/Pt molar ratios of 1/2, 2/2, and 3/2 show a complete reduction 13 of Pt. This can be seen by the linear relationship between the volume of silver nitrate and the Ag/Pt 14 molar ratio for all the samples with a Ag/Pt molar ratio above 1/2. Thus, AA is not only reducing 15 Ag⁺ but is also reducing PtCl₄²⁻. 16 When HQ is used as the reducing agent, using Ag/Pt=1/2 and the associated thin Ag shell, the 17 HQ shows some reduction capability to form some fuzzy spikes (Figure 3a). However, in all the 18 samples using HQ, the galvanic replacement reactions dominate and hence all the samples have a 19 hollow shell structure. In addition, since the HQ has weak or no reducing capability in this context, the Ag⁺ generated via galvanic reaction will form AgCl with Cl⁺ (reaction (4)) when the 20 21 concentrations of ions are high enough. The representative SEM image of the sample with highest 22 molar ratio (Ag/Pt=20/2) fabricated with HQ (Figure 8c), shows very clear AgCl crystals (one 23 example is indicated by the yellow box) and this yellow box area was also investigated via

- 1 conducted EDX which further confirms that the observed crystal is formed from the elements Ag
- 2 and Cl (Figure 8d and Figure S9b).

8

9

10

11

12

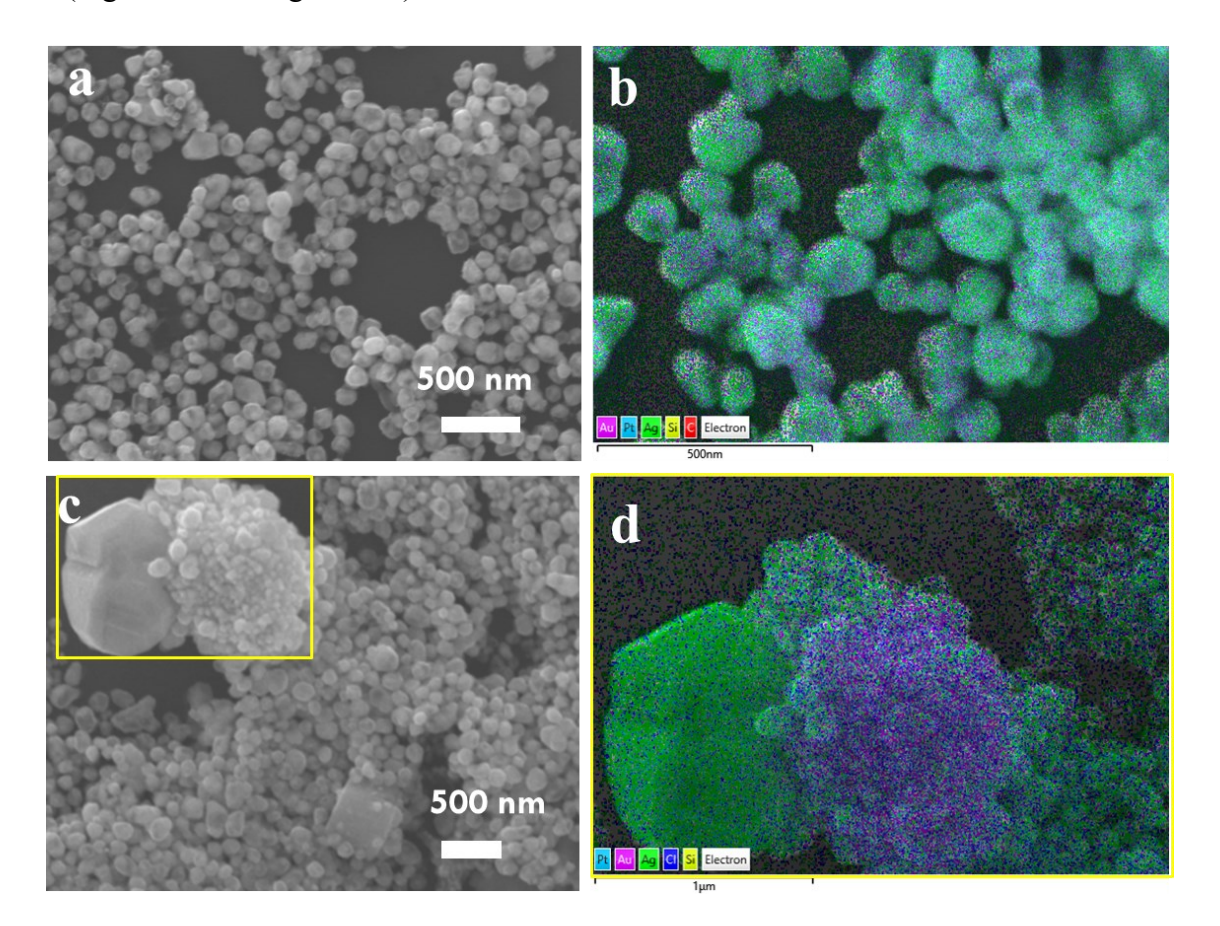


Figure 8. (a) SEM image of sample with highest molar ratio (Ag/Pt=20/2) prepared under

AA assisted GRR; (b) EDX mapping layered image of sample in (a); (c) SEM image of

sample with highest molar ratio (Ag/Pt=20/2) prepared under HQ assisted GRR; (d) EDX

7 mapping layered image of sample in (a) roughly at highlight yellow box.

Catalytic reduction of 4-NP using fabricated catalysts. Nitrophenols (NPs), including para-, meta- and ortho-nitrophenol are one kind of hazardous and toxic pollutant derived from the manufacture of pesticides, pharmaceutical and synthetic dyes.⁶⁴⁻⁶⁵ It is critical to remove the soluble and stable nitrophenols efficiently and completely from wastewater. In addition, the reduction of 4-nitrophenol (4-NP) by NaBH₄ in an aqueous solution is a well-known and easily

monitored reaction. Thus, it was chosen as a model reaction to test the catalytic activity of the fabricated nanomaterials. 66-67 The reaction, as the insert in Figure 9, monitored by collecting the UV-visible absorption spectrum of the mixture of 4-NP and NaBH₄ at different times. As an example, Figure 9 shows time-dependent UV-Vis absorption spectra of the 4-NP solution (3 mM, 100 μL) mixed with 100 μL as-purified nanocatalysts in 2.8 mL nanopure water. Each spectrum was recorded two minutes after the prior spectrum. Initially, the solution showed absorption peak at ~400 nm due to the formation of 4-nitrophenolate ions which is caused by the addition of NaBH₄ solutions. With the addition of catalyst, the absorption peak at ~400 nm decreases and a new peak at 315 nm associated with -NH₂ of 4-aminophenol (4-AP), appeared and increased with reaction time, which demonstrates that the 4-NP has been rapidly and effectively reduced to 4-AP under the acceleration of catalysts. During the reaction, the presence of NaBH₄ in nitrophenols solution resulted in the deprotonation of nitrophenols to nitrophenolate ions which were adsorbed on the surface of catalyst via nitro groups. The electrons generated from the reaction of BH⁴⁻ and H⁺ transferred to nitrophenolate ions through the unique electronic structure of nanostructure, and the nitrophenolate ions received electrons to form aminophenols. The kinetic reaction rate (k) could be evaluated by a pseudo-firstorder kinetics which could be estimated from the plot of $ln(A_0/A_t)$ versus the reaction time, in which A is the absorption at 400 nm, while A₀ and A_t are the absorbance at the initial stage and successive intervals, respectively.

1

2

3

4

5

6

7

8

9

10

11

12

13

14

15

16

17

18

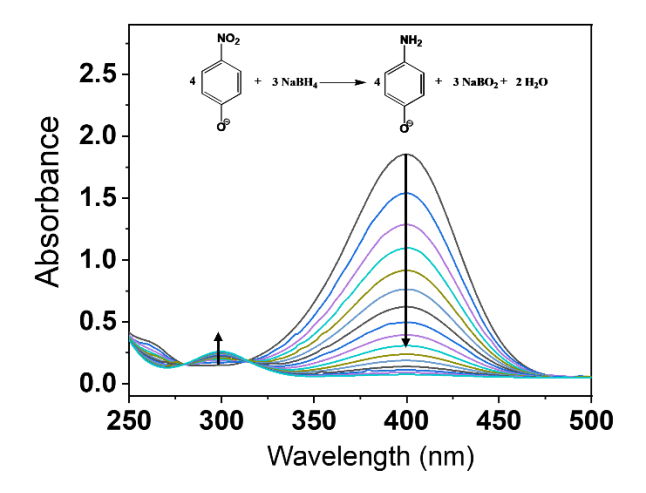


Figure 9. Time dependent UV-vis absorption spectra of 4-NP reduced by NaBH₄ and catalyzed by the Pt based metallic catalysis.

Catalytical performance of fabricated nanocatalysts. Figure S11 and S12 show the representative time-dependent UV-Vis absorption spectra of the 4-NP solution mixed with all the nanocatalysts obtained with each of HQ and AA. $Ln(A_0/A_1)$ as a function of reaction time for all the structures are depicted to facilitate direct comparison of catalytic activity between those nanostructures. The same catalytic reactions were repeated more than 5 times to get more reliable data. The average rate of each reaction can be plotted using the linear fit equation $ln(A_0/A_1)$ =kt. Figure 10a shows a representative plot of $ln(A_0/A_1)$ as a function of reaction time for all the structures fabricated with HQ. With increased volume of AgNO3, the reaction rate is gradually increased. The samples made with the largest amount of AgNO3, 120 μ L and 200 μ L, have very similar reaction rates, as shown by the blue and pink triangles in Figure 10a, indicating that it has reached the catalytic activity plateau. Figure 10b plots the average reaction rate as a function of AgNO3 volume. Consistent with Figure 10a, the average rate increases gradually with increasing AgNO3 volume until the volume of AgNO3 is up to approximately 100 μ L and such trend can be nicely fit with an exponential growth curve. This indicates that the catalysis performance increases

- as the shell volume increases and eventually reaches a plateau. This is not surprising since the
- 2 hollow shell structure is graduated enlarged which increases the total surface area along with the
- 3 number of potential reaction sites which will enhance the catalytic activity. 68-69

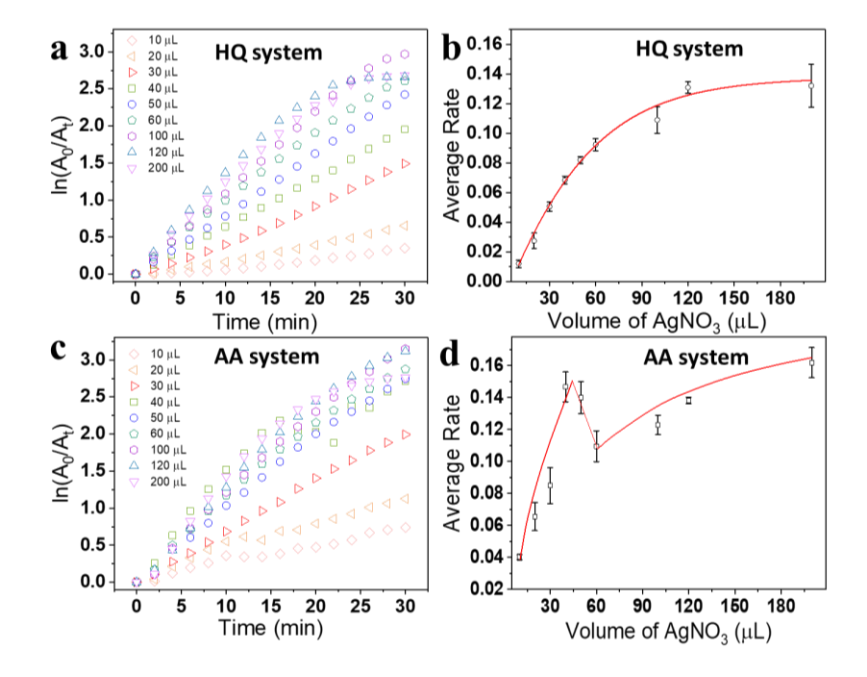


Figure 10. (a) Graph of ln(A₀/A_t) as a function of reaction time giving the comparative rate constants of all the structures fabricated with HQ. (b) Plot of the average reaction rate as a function of the amount of AgNO₃ that was used for the nanocatalyst fabricated with HQ. (c) Graph of ln(A₀/A_t) as a function of reaction time giving the comparative rate constants of all the structures fabricated with AA. (d) Plot of the average reaction rate as a function of the amount of AgNO₃ that was used for the nanocatalyst fabricated with AA.

For the nanocatalysts synthesized with AA, $\ln(A_0/A_t)$ as a function of reaction time is depicted in Figure 10c. The average reaction rate value as a function of AgNO₃ volume is plotted in Figure 10d. It provides a clear trend on how the reaction rate changes over the AgNO₃ volume range. At the beginning, the reaction rate has dramatically increased up to samples made in 40 μ L of AgNO₃ volume. Such increased catalytic activity is possible as a result of the increased surface area,

chemical composition, and the morphology from formed spiky branches for those samples. 70-75 However, such spiky branches start to decrease around the nanocatalysts made with 50 μL AgNO₃ which results in the decreased catalytic activity. With the further increased AgNO₃ volume, the hollow shell structure is gradually enlarged while the overall surface area continues to increase, resulting in increased catalytic activity. In addition, the catalytic activity could also be impacted by the absorbed ligands on the surface of catalysis material. It has been reported that citric acid can significantly improve the Pt monolayer shell as the absorbing surfactant during the reaction by the Shao group. ⁷⁶ Thus, future study into if the AA acting as surfactant plays a significant role in

CONCLUSIONS

catalytic activity would be desirable.

In summary, a mesoporous silica (mSiO₂) shell supported gold nanodumbell (AuNDB) nanostructure was first synthesized using seeds for silver shell deposition. Due to the porous structure of mSiO₂, silver ions were able to penetrate through the shell of silica and deposit on the Au surface forming AuNDB@Ag@mSiO₂. The Ag deposition behavior and impacts on nanostructure properties when using various amount of Ag⁺ were discussed. With the fabricated AuNDB@Ag@mSiO₂ nanostructures, hydroquinone and ascorbic acid were used separately to assist the galvanic replacement reaction between the Pt precursor and the Ag sacrificial template. With various thickness of silver shells and the varying strength of the reducing agent, the rates of co-reduction and galvanic replacement reactions in each system could be manipulated, impacting the final morphology and composition of the Pt based catalysts. This catalysis study suggests that the total surface area and the composition of the Ag/Pt alloy can influence the reactivity significantly. Our work advances the rational design of efficient, low-cost catalysts for redox processes.

EXPERIMENTAL SECTION

1

2 Materials. Hexadecyltrimethylammonium bromide (CTAB), gold (III) chloride trihydrate 3 (HAuCl₄·3H₂O), potassium platinum(II) chloride (K₂PtCl₄), potassium iodide (KI), L-ascorbic 4 acid (L-AA), hydroquinone (HQ), sodium borohydride (NaBH₄), polyvinylpyrrolidone (PVP, 5 MW: 55,000), sodium citrate, tetraethyl orthosilicate (TEOS), ammonium hydroxide (NH₄OH), 4-6 nitrophenol (4-NP), and ethanol (EtOH) were all purchased from Sigma-Aldrich. Silver nitrate 7 (AgNO₃) was purchased from Fisher Scientific. All chemicals were used as received without 8 further purification. 9 Synthesis of Gold Nanodumbbells (AuNDBs). The synthesis method via the iodide-mediated 10 growth of AuNDBs is obtained following the protocol with slight modification from the Liz-Marzán group. 49 The starting GNRs were synthesized via a slight modification to the seed 11 12 mediated growth method. 13 To prepare the seeds, 0.250 mL of 0.01 M HAuCl₄ was added to 10.0 mL of 0.1 M CTAB. 0.600 14 mL of 0.01 M NaBH₄ was then added. The solution color changed from orange to light brown, 15 indicating the formation of gold seeds. The solution was stirred for 2 min and left to stand for 2 16 hrs. For the growth solution, a solution of surfactants was first prepared by dissolving 1.445 g of 17 CTAB into 40 mL nanopure water at 45 °C and cool to room temperature before use. Then, 2.0 18 mL of 0.01 M HAuCl₄ and 0.800 mL of 1 M HCl were added to the surfactant solution and shaken 19 for 30 seconds. This was followed by the addition of 0.400 mL of 0.01 M AgNO₃ and 0.320 mL 20 of 0.1 M L-AA and shaken for another 30 seconds. Finally, 0.096 mL of Au seed solution was 21 added and the solution was shaken for 30 seconds and then left in a 35 °C water bath for at least 22 16 hrs for the completion of gold nanorods growth.

- In order to synthesis AuNDBs, the 10 mL as-synthesized gold nanorods were centrifuged and
- 2 washed twice in nanopure water at 11,000 rpm for 8 min. Then the purified gold nanorods were
- 3 redispersed in a 2 mL, 10 mM aqueous CTAB solution for further use.
- 4 A solution was prepared by mixing 10.0 mL, 10 mM CTAB aqueous CTAB and 50 μL, 0.05 M
- 5 HAuCl₄·3H₂O. The solution was kept at room temperature for 5 min before adding 5.7 μL, 0.01
- 6 M KI and 40 μL, 0.1 M L-AA. Finally, 600 μL of gold nanorods that prepared earlier was then
- 7 added into the mixture solution under stirring. The whole solution was stirred for 1 hour. The
- 8 resultant AuNDBs were centrifuged and redispersed in nanopure water at 8,000 rpm for 8 min
- 9 before silica shell coating or further characterization.
- 10 Synthesis of Silica Coated AuNDBs (AuNDBs@SiO2). The as-synthesized AuNDBs were
- centrifuged at 8,000 rpm for 8 min, and the precipitates were redispersed in an aqueous CTAB
- solution (10 mL, 9 mM). Under gentle stirring, aqueous NH₄OH (150 μL, 0.01 M) was added to
- adjust pH to 10.4, followed by three sequential additions of TEOS in EtOH (10 μL, 20 % (v/v))
- with 30 min intervals in between additions. The solution was then left under stirring conditions for
- 15 24 h at room temperature. The as-prepared AuNDBs@SiO₂ were centrifuged and washed twice in
- 16 EtOH at 8,000 rpm for 8 min. After that, the sample was ready for the deposition of Ag shell and
- 17 further characterization. With the presented amount of TEOS, the formed mSiO₂ shell thickness is
- approximately 19 nm, which was measured on either side of AuNDBs.
- 19 Preparation of Silica Coated AuNDBs-Ag Core-Shell (AuNDBs@Ag@SiO2). The as-
- purified AuNDBs@SiO₂ (1 mL) was dispersed in an aqueous PVP solution (1 mL, 70.4 mg).
- Under stirring, various volumes of 0.01M AgNO₃ (10 μ L, 20 μ L, 30 μ L, 40 μ L, 50 μ L, 60 μ L,
- 100μ L, 120μ L, and 200μ L) were added, followed by the addition of HQ (140 μL, 0.01 M) and
- 23 allowed to stir for 1 h and sat undisturbed for 12 h. The solution was then centrifuged and washed

- 1 twice in EtOH at 8,000 rpm for 8 min before the deposition of Pt shell and characterization. The
- 2 calculated Au/Ag molar ratio is 15/x, (x=1, 2, 3, 4, 5, 6, 10, 12, 20).
- 3 Preparation of Silica Coated AuNDBs@Pt@SiO₂ Nanocatalysts. After the initial purification
- 4 of AuNDBs@Ag@SiO₂ at various volumes of AgNO₃, the precipitate was dispersed in an aqueous
- 5 PVP solution (1 mL, 70.4 mg). Under stirring, K₂PtCl₄ (20 μL, 0.01 M) and two different reducing
- 6 agents, L-AA (40 μL, 0.1 M) and HQ (40 μL, 0.01 M), were added to yield different morphological
- 7 nanocatalysts. The solution was stirred for 5 min and sat undisturbed for 12 h. The solution was
- 8 then centrifuged and washed twice in nanopure water at 8,000 rpm for 8 min before the catalytic
- 9 reduction of 4-nitrophenol and any characterization. The calculated Ag/Pt molar ratio is x/2, (x=1,
- 10 2, 3, 4, 5, 6, 10, 12, 20).
- 11 Catalytic Reduction of 4-Nitrophenol. The catalytic properties of silica coated hollow
- 12 AuNDBs@Pt nanocatalysts were studied by in situ UV-Vis monitoring the change in absorption
- of 4-NP in the presence of NaBH₄ at 400 nm. In a typical catalysis experiment, nanopure water
- 14 (2.8 mL) was added into a quartz cuvette, followed by the addition of an aqueous solution of 4-NP
- 15 (100 μL, 0.003 M) and the as-purified AuNDBs@Pt@SiO₂ nanocatalysts (100 μL). Upon
- beginning in situ monitoring, freshly prepared ice cold NaBH₄ (100 μL, 0.3 M) was added. The
- catalytic reduction was monitored by observing the change in absorption at a wavelength peak of
- 18 400 nm with a 1 min interval over a span of 30 min with the use of the UV-Visible
- 19 spectrophotometer.
- 20 **Instruments and measurement.** Scanning transmission electron microscopy (STEM) imaging,
- 21 energy dispersive X-ray spectroscopy (EDX) and elemental mapping were conducted using a
- JOEL-7200F field emission SEM operated at 30 kV. Higher resolution TEM (HRTEM) images,
- 23 high resolution EDX mapping of individual nanostructure were obtained using a FEI Tecnai F20

- 1 instrument (Thermo Fisher Scientific) operated at 200 kV. The XPS measurements were
- 2 performed on a Surface Science Instruments M Probe ESCA spectrometer with a 200 watt
- 3 monochromatic Al Kα x-ray source, hemispherical analyzer, and a take-off angle of 55° with
- 4 respect to vertical. All the material sizes were measured via STEM images by ImageJ software.
- 5 The STEM samples were prepared by drop casting samples onto copper grids. UV-Vis absorption
- 6 spectra were measured using a Jasco V 670 UV-Vis-NIR spectrophotometer.
- 7 ASSOCIATED CONTENT
- **8** Supporting Information.

11

12

13

14

15

16

17

18

19

20

21

22

- 9 The Supporting Information is available free of charge.
 - Detailed discussion on the possible mechanism of fabricating AuNDBs by using AuNRs; **UV-Vis** of AuNRs, AuNDB, AuNDB@mSiO₂ absorption spectra AuNDB@Ag@mSiO₂ and their spectra change discussion; the UV-Vis spectra of nanostructure before and after the galvanic reaction using HQ coupled GRR between Pt precursor and silver shell which is from the AuNDB@Ag@mSiO₂ made with 20 μL of AgNO₃; representative STEM images of HQ assisted Pt based nanocatalysis using AuNDB@Ag@mSiO₂ made with various amount of AgNO₃; the UV-Vis spectra of nanostructure before and after the galvanic reaction using AA coupled GRR between Pt precursor and silver shell which is from the AuNDB@Ag@mSiO₂ made with 20 μL of AgNO₃; HRTEM image and lattice fringe of AA assisted Pt based nanocatalysis using AuNDB@Ag@mSiO₂ under GRR; XPS spectrum of Ag 3d and Pt 4d of AA assisted Pt based nanocatalysis using AuNDB@Ag@mSiO₂ made with 30 μL of AgNO₃ (Ag/Pt=3/2); representative STEM images of AA assisted Pt based nanocatalysis using AuNDB@Ag@mSiO2 made with various amount of AgNO3; the reaction kinetic UV-

1 visible spectra of forming samples with molar ratio of Ag/Pt = 3/2, 5/2 and the summarized 2 peak intensity value change plots as the function of reaction time; EDX spectra of samples 3 with highest molar ratio (Ag/Pt=20/2) prepared under AA or HQ assisted GRR; the plot of 4 Ag/Pt atomic ratio as the function of the silver nitrate volume with AA as reducing agent; 5 the representative time-dependent UV-Vis absorption spectra of the 4-NP solution mixed 6 with all the nanocatalysts obtained with HQ and AA. 7 **AUTHOR INFORMATION** 8 **Corresponding Author** 9 *Ying Bao — Department of Chemistry, Western Washington University, Bellingham, 98225, 10 WA, USA; Email: ying.bao@wwu.edu 11 **Authors** 12 **John R. Crockett** — Department of Chemistry, Western Washington University, Bellingham, 13 98225, WA, USA; 14 **Maggie Wang** — Department of Chemistry, Western Washington University, Bellingham, 15 98225, WA, USA; 16 **Joseph E. Doebler** — Department of Chemistry, Western Washington University, Bellingham, 98225, WA, USA; 17 18 **Tejal Pawale** — *Materials Science and Engineering Department, University of North Texas,* 19 Denton, TX 76207, USA; 20 **Xiao Li** — Materials Science and Engineering Department, University of North Texas, 21 Denton, TX 76207, USA; 22 **Notes** 23 The authors declare no competing financial interest. 24 ACKNOWLEDGMENT 25 This research was supported by Western Washington University, Department of Chemistry. 26 STEM studies were conducted on an instrument funded by the Joint Center for Deployment and 27 Research in Earth Abundant Materials (JCDREAM). J. R. C.'s contributions were partially

- supported by the National Science Foundation (grant no. 2108842). J. E. D. thanks the partial
- 2 support from the RSP graduate award from Western Washington University. The authors are
- 3 grateful to Alexandra Hoff and Bryce Pettit Estell for their help on data analysis, as well as all
- 4 members in Bao group for valuable discussions.

REFERENCES

- 6 1. Moiseev, I. I., Catalysis: 2000 AD1. Kinet. Catal. 2001, 42 (1), 1-22.
- 7 2. Voltz, S. E.; Morgan, C. R.; Liederman, D.; Jacob, S. M., Kinetic Study of Carbon
- 8 Monoxide and Propylene Oxidation on Platinum Catalysts. *Product R&D* **1973,** *12* (4), 294-301.
- 9 3. Gasteiger, H. A.; Kocha, S. S.; Sompalli, B.; Wagner, F. T., Activity benchmarks and
- 10 requirements for Pt, Pt-alloy, and non-Pt oxygen reduction catalysts for PEMFCs. Appl. Catal., B
- 11 **2005,** *56* (1), 9-35.
- 12 4. Burch, R.; Breen, J. P.; Meunier, F. C., A review of the selective reduction of NOx with
- 13 hydrocarbons under lean-burn conditions with non-zeolitic oxide and platinum group metal
- 14 catalysts. Appl. Catal., B **2002**, 39 (4), 283-303.
- 15 5. Li, L.; Larsen, A. H.; Romero, N. A.; Morozov, V. A.; Glinsvad, C.; Abild-Pedersen, F.;
- 16 Greeley, J.; Jacobsen, K. W.; Nørskov, J. K., Investigation of Catalytic Finite-Size-Effects of
- 17 Platinum Metal Clusters. *J. Phys. Chem. Lett* **2013**, *4* (1), 222-26.
- Lopes, P. P.; Li, D.; Lv, H.; Wang, C.; Tripkovic, D.; Zhu, Y.; Schimmenti, R.; Daimon,
- 19 H.; Kang, Y.; Snyder, J.; Becknell, N.; More, K. L.; Strmcnik, D.; Markovic, N. M.; Mavrikakis,
- 20 M.; Stamenkovic, V. R., Eliminating dissolution of platinum-based electrocatalysts at the atomic
- 21 scale. Nat. Mater. 2020, 19 (11), 1207-14.
- 22 7. Liang, Z.; Song, L.; Elnabawy, A. O.; Marinkovic, N.; Mavrikakis, M.; Adzic, R. R.,
- 23 Platinum and Palladium Monolayer Electrocatalysts for Formic Acid Oxidation. *Top. Catal.*
- 24 **2020,** *63* (7), 742-49.
- 25 8. Yang, L.; Vukmirovic, M. B.; Su, D.; Sasaki, K.; Herron, J. A.; Mavrikakis, M.; Liao, S.;
- Adzic, R. R., Tuning the Catalytic Activity of Ru@Pt Core—Shell Nanoparticles for the Oxygen
- 27 Reduction Reaction by Varying the Shell Thickness. The Journal of Physical Chemistry C 2013,
- 28 117 (4), 1748-53.
- 29 9. Yuan, Q.; Wakisaka, Y.; Uemura, Y.; Wada, T.; Ariga-Miwa, H.; Takakusagi, S.;
- 30 Asakura, K.; Brankovic, S. R., Reaction Stoichiometry and Mechanism of Pt Deposition via
- 31 Surface Limited Redox Replacement of Copper UPD Layer on Au(111). The Journal of Physical
- 32 *Chemistry C* **2018,** *122* (29), 16664-73.
- 33 10. Xie, Y.; Yang, Y.; Muller, D. A.; Abruña, H. D.; Dimitrov, N.; Fang, J., Enhanced ORR
- Kinetics on Au-Doped Pt–Cu Porous Films in Alkaline Media. ACS Catalysis 2020, 10 (17),
- 35 9967-76.
- 36 11. Xie, Y.; Li, C.; Razek, S. A.; Fang, J.; Dimitrov, N., Synthesis of Nanoporous Au–Cu–Pt
- 37 Alloy as a Superior Catalyst for the Methanol Oxidation Reaction. ChemElectroChem 2020, 7
- 38 (2), 569-80.
- 39 12. Xie, Y.; Dimitrov, N., Ultralow Pt loading nanoporous Au-Cu-Pt thin film as highly
- 40 active and durable catalyst for formic acid oxidation. *Appl. Catal.*, B **2020**, 263, 118366.

- 1 13. Yuan, Q.; Doan, H. A.; Grabow, L. C.; Brankovic, S. R., Finite Size Effects in
- 2 Submonolayer Catalysts Investigated by CO Electrosorption on PtsML/Pd(100). J. Am. Chem.
- 3 *Soc.* **2017,** *139* (39), 13676-79.
- 4 14. Pizzutilo, E.; Geiger, S.; Grote, J. P.; Mingers, A.; Mayrhofer, K. J. J.; Arenz, M.;
- 5 Cherevko, S., On the Need of Improved Accelerated Degradation Protocols (ADPs):
- 6 Examination of Platinum Dissolution and Carbon Corrosion in Half-Cell Tests. J. Electrochem.
- 7 *Soc.* **2016,** *163* (14), F1510-F14.
- 8 15. Shao-Horn, Y.; Sheng, W. C.; Chen, S.; Ferreira, P. J.; Holby, E. F.; Morgan, D.,
- 9 Instability of Supported Platinum Nanoparticles in Low-Temperature Fuel Cells. *Top. Catal.*
- 10 **2007,** *46* (3), 285-305.
- 11 16. Ferreira, P. J.; la O', G. J.; Shao-Horn, Y.; Morgan, D.; Makharia, R.; Kocha, S.;
- Gasteiger, H. A., Instability of Pt / C Electrocatalysts in Proton Exchange Membrane Fuel Cells.
- 13 J. Electrochem. Soc. 2005, 152 (11), A2256.
- 14 17. de Bruijn, F. A.; Dam, V. A. T.; Janssen, G. J. M., Review: Durability and Degradation
- 15 Issues of PEM Fuel Cell Components. Fuel Cells 2008, 8 (1), 3-22.
- 16 18. Bai, L.; Wang, X.; Chen, Q.; Ye, Y.; Zheng, H.; Guo, J.; Yin, Y.; Gao, C., Explaining the
- 17 Size Dependence in Platinum-Nanoparticle-Catalyzed Hydrogenation Reactions. *Angew. Chem.*
- 18 *Int. Ed.* **2016,** *55* (50), 15656-61.
- 19 19. Lee, H.; Habas, S. E.; Kweskin, S.; Butcher, D.; Somorjai, G. A.; Yang, P.,
- 20 Morphological Control of Catalytically Active Platinum Nanocrystals. *Angew. Chem. Int. Ed.*
- 21 **2006,** *45* (46), 7824-28.
- 22 20. Narayanan, R.; El-Sayed, M. A., Shape-Dependent Catalytic Activity of Platinum
- Nanoparticles in Colloidal Solution. *Nano Lett.* **2004,** *4* (7), 1343-48.
- 24 21. Tominaka, S.; Nakamura, Y.; Osaka, T., Nanostructured catalyst with hierarchical
- porosity and large surface area for on-chip fuel cells. J. Power Sources 2010, 195 (4), 1054-58.
- 26 22. Xiao, M.; Wang, Z.; Lyu, M.; Luo, B.; Wang, S.; Liu, G.; Cheng, H.-M.; Wang, L.,
- 27 Hollow Nanostructures for Photocatalysis: Advantages and Challenges. Adv. Mater. 2019, 31
- 28 (38), 1801369.
- 29 23. Cohen-Pope, S.; Crockett, J. R.; Wang, M.; Flynn, K.; Hoff, A.; Bao, Y., Morphology
- control of SERS-active 2D gold nanosnowflakes. J. Mater. Chem. C 2020, 8 (36), 12427-36.
- 31 24. Alayoglu, S.; Nilekar, A. U.; Mavrikakis, M.; Eichhorn, B., Ru–Pt core–shell
- nanoparticles for preferential oxidation of carbon monoxide in hydrogen. *Nat. Mater.* **2008**, 7
- 33 (4), 333-38.
- 34 25. Wang, J.; Loh, K. P.; Zhong, Y. L.; Lin, M.; Ding, J.; Foo, Y. L., Bifunctional FePt
- 35 Core-Shell and Hollow Spheres: Sonochemical Preparation and Self-Assembly. *Chem. Mater.*
- **2007,** *19* (10), 2566-72.
- 26. Zeng, J.; Yang, J.; Lee, J. Y.; Zhou, W., Preparation of Carbon-Supported Core-Shell
- 38 Au–Pt Nanoparticles for Methanol Oxidation Reaction: The Promotional Effect of the Au Core.
- 39 J. Phys. Chem. B 2006, 110 (48), 24606-11.
- 40 27. Ruditskiy, A.; Choi, S.-I.; Peng, H.-C.; Xia, Y., Shape-controlled metal nanocrystals for
- 41 catalytic applications. MRS Bull. **2014**, *39* (8), 727-37.
- 42 28. Chen, S.; Thota, S.; Singh, G.; Aímola, T. J.; Koenigsmann, C.; Zhao, J., Synthesis of
- 43 hollow Pt–Ag nanoparticles by oxygen-assisted acid etching as electrocatalysts for the oxygen
- 44 reduction reaction. *RSC Advances* **2017,** *7* (74), 46916-24.

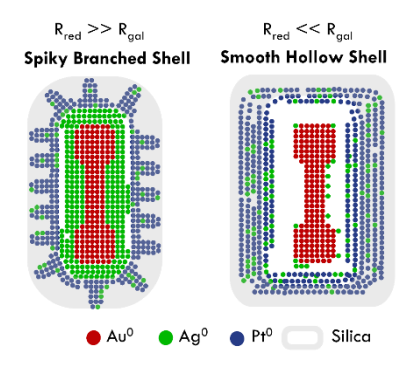
- 1 29. Chen, S.; Thota, S.; Wang, X.; Zhao, J., From solid to core@shell to hollow Pt-Ag
- 2 nanocrystals: thermally controlled surface segregation to enhance catalytic activity and
- 3 durability. J. Mater. Chem. A **2016**, 4 (23), 9038-43.
- 4 30. Tan, C.; Sun, Y.; Zheng, J.; Wang, D.; Li, Z.; Zeng, H.; Guo, J.; Jing, L.; Jiang, L., A
- 5 self-supporting bimetallic Au@Pt core-shell nanoparticle electrocatalyst for the synergistic
- 6 enhancement of methanol oxidation. Sci. Rep. 2017, 7 (1), 6347.
- 7 31. Singh, B.; Seddon, B.; Dempsey, E.; Redington, W.; Dickinson, C., Porous Core-Shell
- 8 Platinum-Silver Nanocatalyst for the Electrooxidation of Methanol. *Electroanalysis* **2015**, *27* (1),
- 9 135-43.
- 10 32. R. Daniel, J.; McCarthy, L. A.; Ringe, E.; Boudreau, D., Enhanced control of plasmonic
- properties of silver–gold hollow nanoparticles via a reduction-assisted galvanic replacement
- 12 approach. RSC Advances **2019**, 9 (1), 389-96.
- 13 33. Xia, X.; Wang, Y.; Ruditskiy, A.; Xia, Y., 25th Anniversary Article: Galvanic
- 14 Replacement: A Simple and Versatile Route to Hollow Nanostructures with Tunable and Well-
- 15 Controlled Properties. *Adv. Mater.* **2013**, *25* (44), 6313-33.
- 16 34. Sun, Y.; Xia, Y., Shape-Controlled Synthesis of Gold and Silver Nanoparticles. *Science*
- 17 **2002,** *298* (5601), 2176-79.
- Wiley, B.; Sun, Y.; Chen, J.; Cang, H.; Li, Z.-Y.; Li, X.; Xia, Y., Shape-Controlled
- 19 Synthesis of Silver and Gold Nanostructures. MRS Bull. 2005, 30 (5), 356-61.
- 20 36. Bansal, V.; O'Mullane, A.; Bhargava, S., Galvanic replacement mediated synthesis of
- 21 hollow Pt nanocatalysts: Significance of residual Ag for the H 2 evolution reaction. *Electrochem*.
- 22 *Commun.* **2009**, *11* (8), 1639-42.
- 23 37. Yang, X.; Roling, L. T.; Vara, M.; Elnabawy, A. O.; Zhao, M.; Hood, Z. D.; Bao, S.;
- 24 Mavrikakis, M.; Xia, Y., Synthesis and Characterization of Pt–Ag Alloy Nanocages with
- Enhanced Activity and Durability toward Oxygen Reduction. *Nano Lett.* **2016**, *16* (10), 6644-49.
- 26 38. Chen, J.; Wiley, B.; McLellan, J.; Xiong, Y.; Li, Z.-Y.; Xia, Y., Optical Properties of
- 27 Pd-Ag and Pt-Ag Nanoboxes Synthesized via Galvanic Replacement Reactions. *Nano Lett.*
- 28 **2005,** *5* (10), 2058-62.
- 29 39. Lee, C.-L.; Tseng, C.-M., Ag-Pt Nanoplates: Galvanic Displacement Preparation and
- Their Applications As Electrocatalysts. J. Phys. Chem. C. 2008, 112 (35), 13342-45.
- 31 40. Zhang, W.; Yang, J.; Lu, X., Tailoring Galvanic Replacement Reaction for the
- 32 Preparation of Pt/Ag Bimetallic Hollow Nanostructures with Controlled Number of Voids. ACS
- 33 *Nano* **2012,** *6* (8), 7397-405.
- 34 41. Zhang, H.; Jin, M.; Wang, J.; Li, W.; Camargo, P. H. C.; Kim, M. J.; Yang, D.; Xie, Z.;
- 35 Xia, Y., Synthesis of Pd–Pt Bimetallic Nanocrystals with a Concave Structure through a
- Bromide-Induced Galvanic Replacement Reaction. J. Am. Chem. Soc. 2011, 133 (15), 6078-89.
- 37 42. Ye, F.; Liu, H.; Hu, W.; Zhong, J.; Chen, Y.; Cao, H.; Yang, J., Heterogeneous Au–Pt
- nanostructures with enhanced catalytic activity toward oxygen reduction. Dalton Trans. 2012, 41
- 39 (10), 2898-903.
- 40 43. Merkoçi, F.; Patarroyo, J.; Russo, L.; Piella, J.; Genç, A.; Arbiol, J.; Bastús, N. G.;
- 41 Puntes, V., Understanding galvanic replacement reactions: the case of Pt and Ag. *Mater. Today*
- 42 *Adv.* **2020,** *5*, 100037.
- 43 44. Bordley, J. A.; El-Sayed, M. A., Enhanced Electrocatalytic Activity toward the Oxygen
- 44 Reduction Reaction through Alloy Formation: Platinum–Silver Alloy Nanocages. J. Phys. Chem.
- 45 *C.* **2016,** *120* (27), 14643-51.

- 1 45. Rodrigues, T. S.; da Silva, A. G. M.; Gonçalves, M. C.; Fajardo, H. V.; Balzer, R.;
- 2 Probst, L. F. D.; Camargo, P. H. C., AgPt Hollow Nanodendrites: Synthesis and Uniform
- 3 Dispersion over SiO2 Support for Catalytic Applications. *ChemNanoMat* **2015**, *1* (1), 46-51.
- 4 46. Rodrigues, T. S.; da Silva, A. H. M.; da Silva, A. G. M.; Ceara, D. G.; Gomes, J. F.;
- 5 Assaf, J. M.; Camargo, P. H. C., Hollow AgPt/SiO2 nanomaterials with controlled surface
- 6 morphologies: is the number of Pt surface atoms imperative to optimize catalytic performances?
- 7 *Catal. Sci. Technol.* **2016,** *6* (7), 2162-70.
- 8 47. Crockett, J. R.; Win-Piazza, H.; Doebler, J. E.; Luan, T.; Bao, Y., Plasmonic Detection of
- 9 Mercury via Amalgamation on Gold Nanorods Coated with PEG-Thiol. ACS Appl. Nano Mater.
- 10 **2021,** *4* (2), 1654-63.
- Wang, M.; Hoff, A.; Doebler, J. E.; Emory, S. R.; Bao, Y., Dumbbell-Like Silica Coated
- Gold Nanorods and Their Plasmonic Properties. *Langmuir* **2019**, *35* (51), 16886-92.
- 49. Grzelczak, M.; Sánchez-Iglesias, A.; Rodríguez-González, B.; Alvarez-Puebla, R.; Pérez-
- Juste, J.; Liz-Marzán, L. M., Influence of Iodide Ions on the Growth of Gold Nanorods: Tuning
- 15 Tip Curvature and Surface Plasmon Resonance. Adv. Funct. Mater. 2008, 18 (23), 3780-86.
- 16 50. Fernanda Cardinal, M.; Rodríguez-González, B.; Alvarez-Puebla, R. A.; Pérez-Juste, J.;
- 17 Liz-Marzán, L. M., Modulation of Localized Surface Plasmons and SERS Response in Gold
- 18 Dumbbells through Silver Coating. J. Phys. Chem. C. **2010**, 114 (23), 10417-23.
- 19 51. Tebbe, M.; Kuttner, C.; Mayer, M.; Maennel, M.; Pazos-Perez, N.; König, T. A. F.; Fery,
- 20 A., Silver-Overgrowth-Induced Changes in Intrinsic Optical Properties of Gold Nanorods: From
- 21 Noninvasive Monitoring of Growth Kinetics to Tailoring Internal Mirror Charges. *J Phys Chem*
- 22 C Nanomater Interfaces **2015**, 119 (17), 9513-23.
- 23 52. Gómez-Graña, S.; Goris, B.; Altantzis, T.; Fernández-López, C.; Carbó-Argibay, E.;
- 24 Guerrero-Martínez, A.; Almora-Barrios, N.; López, N.; Pastoriza-Santos, I.; Pérez-Juste, J.; Bals,
- 25 S.; Van Tendeloo, G.; Liz-Marzán, L. M., Au@Ag Nanoparticles: Halides Stabilize {100}
- 26 Facets. J. Phys. Chem. Lett **2013**, 4 (13), 2209-16.
- 53. Sánchez-Iglesias, A.; Carbó-Argibay, E.; Glaria, A.; Rodríguez-González, B.; Pérez-
- Juste, J.; Pastoriza-Santos, I.; Liz-Marzán, L. M., Rapid Epitaxial Growth of Ag on Au
- Nanoparticles: From Au Nanorods to Core-Shell Au@Ag Octahedrons. Chem. Eur. J. 2010, 16
- 30 (19), 5558-63.
- 31 54. Becker, J.; Zins, I.; Jakab, A.; Khalavka, Y.; Schubert, O.; Sönnichsen, C., Plasmonic
- Focusing Reduces Ensemble Linewidth of Silver-Coated Gold Nanorods. *Nano Lett.* **2008**, 8 (6),
- 33 1719-23.
- 34 55. Viswanath, B.; Kundu, P.; Halder, A.; Ravishankar, N., Mechanistic Aspects of Shape
- 35 Selection and Symmetry Breaking during Nanostructure Growth by Wet Chemical Methods. *The*
- *Journal of Physical Chemistry C* **2009**, *113* (39), 16866-83.
- 56. Lai, Y.; Du, G.; Zheng, Z.; Dong, Y.; Li, H.; Kuang, Q.; Xie, Z., Facile synthesis of clean
- 38 PtAg dendritic nanostructures with enhanced electrochemical properties. *Inorganic Chemistry*
- 39 Frontiers **2020**, 7 (5), 1250-56.
- 40 57. Huang, M.; Zhang, H.; Yin, S.; Zhang, X.; Wang, J., PtAg Alloy Nanoparticles
- 41 Embedded in Polyaniline as Electrocatalysts for Formate Oxidation and Hydrogen Evolution.
- 42 ACS Appl. Nano Mater. **2020**, 3 (4), 3760-66.
- 43 58. Sui, N.; Wang, K.; Shan, X.; Bai, Q.; Wang, L.; Xiao, H.; Liu, M.; Colvin, V. L.; Yu, W.
- 44 W., Facile synthesis of hollow dendritic Ag/Pt alloy nanoparticles for enhanced methanol
- 45 oxidation efficiency. *Dalton Trans.* **2017**, *46* (44), 15541-48.

- 1 59. Fu, T.; Fang, J.; Wang, C.; Zhao, J., Hollow porous nanoparticles with Pt skin on a Ag–Pt
- 2 alloy structure as a highly active electrocatalyst for the oxygen reduction reaction. J. Mater.
- 3 Chem. A **2016**, 4 (22), 8803-11.
- 4 60. Kalyan, I.; Pal, T.; Pal, A., Time and temperature dependent formation of hollow gold
- 5 nanoparticles via galvanic replacement reaction of As(0) and its catalytic application. MRS
- 6 *Commun.* **2019,** *9* (1), 270-79.
- 7 61. Xia, X.; Wang, Y.; Ruditskiy, A.; Xia, Y., 25th anniversary article: galvanic replacement:
- 8 a simple and versatile route to hollow nanostructures with tunable and well-controlled properties.
- 9 *Adv. Mater.* **2013,** *25* (44), 6313-33.
- 10 62. Matsui, T.; Kitagawa, Y.; Okumura, M.; Shigeta, Y., Accurate Standard Hydrogen
- 11 Electrode Potential and Applications to the Redox Potentials of Vitamin C and NAD/NADH.
- 12 *The Journal of Physical Chemistry A* **2015**, *119* (2), 369-76.
- 13 63. Yadav, A. P.; Sugawara, Y.; Nishikata, A.; Tsuru, T., Electrochemical Stability and
- Oxidation Mechanism of Carbon Support for PEM Fuel Cell. ECS Transactions 2008, 16 (2),
- 15 2093-99.
- 16 64. Ismail, M.; Khan, M. I.; Khan, S. B.; Akhtar, K.; Khan, M. A.; Asiri, A. M., Catalytic
- 17 reduction of pieric acid, nitrophenols and organic azo dyes via green synthesized plant supported
- 18 Ag nanoparticles. *J. Mol. Liq.* **2018**, *268*, 87-101.
- 19 65. Albukhari, S. M.; Ismail, M.; Akhtar, K.; Danish, E. Y., Catalytic reduction of
- 20 nitrophenols and dyes using silver nanoparticles @ cellulose polymer paper for the resolution of
- waste water treatment challenges. Colloids Surf. A Phyusicochem. Eng. 2019, 577, 548-61.
- 22 66. Iben Ayad, A.; Luart, D.; Ould Dris, A.; Guénin, E., Kinetic Analysis of 4-Nitrophenol
- Reduction by "Water-Soluble" Palladium Nanoparticles. *Nanomaterials* **2020**, *10* (6), 1169.
- 67. Gu, S.; Lu, Y.; Kaiser, J.; Albrecht, M.; Ballauff, M., Kinetic analysis of the reduction of
- 4-nitrophenol catalyzed by Au/Pd nanoalloys immobilized in spherical polyelectrolyte brushes.
- 26 *PCCP* **2015,** *17* (42), 28137-43.
- 27 68. Sun, S.; Li, H.; Xu, Z. J., Impact of Surface Area in Evaluation of Catalyst Activity.
- 28 *Joule* **2018,** *2* (6), 1024-27.
- 29 69. Dignon, G. L.; Zheng, W.; Kim, Y. C.; Mittal, J., Temperature-Controlled Liquid–Liquid
- Phase Separation of Disordered Proteins. ACS Cent. Sci. 2019, 5 (5), 821-30.
- 70. Peng, Z.; You, H.; Yang, H., An Electrochemical Approach to PtAg Alloy
- Nanostructures Rich in Pt at the Surface. Adv. Funct. Mater. 2010, 20 (21), 3734-41.
- 33 71. Jiang, X.; Fu, G.; Wu, X.; Liu, Y.; Zhang, M.; Sun, D.; Xu, L.; Tang, Y., Ultrathin AgPt
- 34 alloy nanowires as a high-performance electrocatalyst for formic acid oxidation. *Nano Research*
- 35 **2018,** *11* (1), 499-510.
- 36 72. Zhao, D.; Wang, Y.-H.; Yan, B.; Xu, B.-Q., Manipulation of Pt∧Ag Nanostructures for
- 37 Advanced Electrocatalyst. J. Phys. Chem. C. **2009**, 113 (4), 1242-50.
- 38 73. Varshney, S.; Bar-Ziv, R.; Zidki, T., On the Remarkable Performance of Silver-based
- 39 Alloy Nanoparticles in 4-Nitrophenol Catalytic Reduction. ChemCatChem 2020, 12 (18), 4680-
- 40 88.
- 41 74. Stephens, I. E. L.; Bondarenko, A. S.; Perez-Alonso, F. J.; Calle-Vallejo, F.; Bech, L.;
- Johansson, T. P.; Jepsen, A. K.; Frydendal, R.; Knudsen, B. P.; Rossmeisl, J.; Chorkendorff, I.,
- Tuning the Activity of Pt(111) for Oxygen Electroreduction by Subsurface Alloying. J. Am.
- 44 *Chem. Soc.* **2011,** *133* (14), 5485-91.
- 45 75. Merrill, N. A.; Nitka, T. T.; McKee, E. M.; Merino, K. C.; Drummy, L. F.; Lee, S.;
- Reinhart, B.; Ren, Y.; Munro, C. J.; Pylypenko, S.; Frenkel, A. I.; Bedford, N. M.; Knecht, M.

- 1 R., Effects of Metal Composition and Ratio on Peptide-Templated Multimetallic PdPt
- 2 Nanomaterials. ACS Appl. Mater. Interfaces 2017, 9 (9), 8030-40.
- 3 76. Zhu, S.; Yue, J.; Qin, X.; Wei, Z.; Liang, Z.; Adzic, R. R.; Brankovic, S. R.; Du, Z.;
- 4 Shao, M., The Role of Citric Acid in Perfecting Platinum Monolayer on Palladium Nanoparticles
- during the Surface Limited Redox Replacement Reaction. J. Electrochem. Soc. 2016, 163 (12),
- 6 D3040-D46.

7 Table of Content/Abstract Graphics



9